



RESEARCH ARTICLE

10.1002/2014GB005075

Key Points:

- Transport of C_{ant} at 7.5°N and 24.5°N Atlantic section from in situ data
- C_{ant} storage rates in the tropical North Atlantic
- C_{ant} air-sea fluxes in the tropical North Atlantic

Correspondence to:

P. Zunino,
pzuninor@ifremer.fr

Citation:

Zunino, P., F. F. Pérez, N. M. Fajar, E. F. Guallart, A. F. Ríos, J. L. Pelegrí, and A. Hernández-Guerra (2015), Transports and budgets of anthropogenic CO_2 in the tropical North Atlantic in 1992–1993 and 2010–2011, *Global Biogeochem. Cycles*, 29, 1075–1091, doi:10.1002/2014GB005075.

Received 28 DEC 2014

Accepted 18 JUN 2015

Accepted article online 22 JUN 2015

Published online 28 JUL 2015

Transports and budgets of anthropogenic CO_2 in the tropical North Atlantic in 1992–1993 and 2010–2011

Patricia Zunino¹, Fiz F. Pérez², Noelia M. Fajar², Elisa F. Guallart³, Aida F. Ríos², Josep L. Pelegrí³, and Alonso Hernández-Guerra¹

¹Instituto de Oceanografía y Cambio Global, Universidad de Las Palmas de Gran Canaria, Las Palmas, Spain, ²Instituto de Investigaciones Mariñas, CSIC, Vigo, Spain, ³Institut de Ciències del Mar, CSIC, Barcelona, Spain

Abstract The meridional transport of anthropogenic CO_2 (C_{ant}) in the tropical North Atlantic (TNA) is investigated using data from transoceanic sections along 7.5°N and 24.5°N, carried out in the early 1990s and 2010s. The net C_{ant} transport across both sections is northward. At 7.5°N, this transport increased from $315 \pm 47 \text{ kmol s}^{-1}$ in 1993 to $493 \pm 51 \text{ kmol s}^{-1}$ in 2010; similarly, across 24.5°N it grew from $530 \pm 46 \text{ kmol s}^{-1}$ in 1992 to $662 \pm 49 \text{ kmol s}^{-1}$ in 2011. These changes result from modifications in the intermediate and deep circulation patterns, as well as from C_{ant} increase within the thermocline waters. In deep waters, lateral advection causes a net C_{ant} input of $112 \pm 60 \text{ kmol s}^{-1}$ ($234 \pm 65 \text{ kmol s}^{-1}$) in 1992–1993 (2010–2011); within these deep waters, the storage rate of C_{ant} is not statistically different from the net C_{ant} input, $139 \pm 21 \text{ kmol s}^{-1}$ ($188 \pm 21 \text{ kmol s}^{-1}$) in 1992–1993 (2010–2011). The C_{ant} increase in deep waters is due to the large injection of C_{ant} across the 24.5°N by the Deep Western Boundary Current and the northward recirculation of North Atlantic Deep Water along 7.5°N. In contrast, a large net C_{ant} output in the upper layer is caused by the Florida Current. Despite this net C_{ant} output, the C_{ant} accumulates at a rate of $215 \pm 24 \text{ kmol s}^{-1}$ ($291 \pm 24 \text{ kmol s}^{-1}$) referenced to year 1993 (2010). From the two C_{ant} budgets, we infer a C_{ant} air-sea flux of $0.23 \pm 0.02 \text{ Pg yr}^{-1}$ in the TNA, much larger than previous estimates.

1. Introduction

The ocean plays an essential regulating role in the Earth's climate, controlling the concentration and distribution of many key properties such as the atmospheric CO_2 . Since the beginning of the industrial revolution, a huge amount of CO_2 has been emitted to the atmosphere, and about one third of this total has been incorporated by the ocean [Khatiwala *et al.*, 2013]. Since natural and human-emitted CO_2 are molecularly indistinguishable, the anthropogenic CO_2 (C_{ant}) in the ocean is defined as the excess of CO_2 in relation to the preindustrial (or natural) levels of CO_2 .

The accumulation of C_{ant} is not homogeneous all over the oceans. The highest C_{ant} storage rate is found in the North Atlantic, chiefly in the subpolar North Atlantic [Sabine *et al.*, 2004; Khatiwala *et al.*, 2013]. This larger C_{ant} accumulation in the North Atlantic is explained by the injection of C_{ant} -enriched water in the ocean interior through ventilation and water formation processes [Rhein *et al.*, 2007; Steinfeldt *et al.*, 2009]. Likewise, the Atlantic Meridional Overturning Circulation (AMOC) is also a supplier of C_{ant} to the North Atlantic, because of its northward transports of C_{ant} -enriched waters along the North Atlantic. Indeed, Pérez *et al.* [2013] found a positive correlation between AMOC intensity and C_{ant} storage rate in the subpolar North Atlantic.

Observational estimates of C_{ant} and ocean circulation models have been combined in inverse schemes to estimate C_{ant} air-sea fluxes, C_{ant} storage rate, and C_{ant} transport in the ocean interior [Mikaloff Fletcher *et al.*, 2006; Gruber *et al.*, 2009; DeVries, 2014]. These estimations, however, need to be validated by observational results. Transport of C_{ant} can be calculated from cruise data by the combination of mass transport and C_{ant} estimates. C_{ant} storage rate is also possible to be computed with in situ data. Unfortunately, direct measurements of C_{ant} air-sea fluxes are not achievable.

Several previous works have appraised the C_{ant} transport in the North Atlantic using cruise data. Rosón *et al.* [2003] computed C_{ant} transport across the 24°N section in 1992 to be $610 \pm 200 \text{ kmol s}^{-1}$. Macdonald *et al.* [2003]

estimated the C_{ant} transport across this same latitude in 1992 and 1998 to be $449 \pm 158 \text{ kmol s}^{-1}$ and $528 \pm 41 \text{ kmol s}^{-1}$, respectively. The transport of C_{ant} across a 1997 section crossing the subpolar North Atlantic (FOUREX section, from Greenland to Portugal) was estimated to be $116 \pm 126 \text{ kmol s}^{-1}$ by *Álvarez et al.* [2003] and $289 \pm 32 \text{ kmol s}^{-1}$ by *Zunino et al.* [2014]. *Zunino et al.* [2014] calculated the mean C_{ant} transport into the subpolar North Atlantic (OVIDE section), for the first decade of the 2000s, as $254 \pm 32 \text{ kmol s}^{-1}$. Some general statements come out from these results. First, there is a reduction in the northward transport of C_{ant} with increasing latitude. Second, for the same latitude and year the results may differ depending on the method used for estimating the velocity and C_{ant} fields. Finally, for the same section, temporal variations in C_{ant} transport may be caused by changes in both C_{ant} concentration and circulation patterns.

In the present work we focus on the tropical North Atlantic (TNA), from 7.5°N to 24.5°N . The transport of C_{ant} across 7.5°N is investigated here for the first time using in situ data. Next, the differences in C_{ant} transport across 7.5°N (24.5°N), between two situations that elapsed 17 (19) years, are exposed. It is worth highlighting that the methods for computing the velocity and C_{ant} fields are exactly the same in all the cases; consequently, the possible differences in C_{ant} transport are exclusively due to changes in C_{ant} concentration and/or circulation patterns.

Recent studies by *Fajar et al.* [2015] and *Guallart et al.* [2015] have analyzed decadal C_{ant} changes for different water masses and regions along 7.5°N and 24.5°N . The changes along 7.5°N have been calculated between 1993 and 2010 by *Fajar et al.* [2015]. An increase in C_{ant} was detected at all depths, with maxima in the thermocline and intermediate waters. A zonal gradient in C_{ant} increase rates was detected, with different behavior depending on the depth in the water column. The greatest C_{ant} increase rate in the thermocline and intermediate waters was found in the eastern margin, while in the deep water it was found in the western margin. *Tanhua et al.* [2006] found, for the North Atlantic Ocean, that changes in C_{ant} concentration through the whole water column are proportional to the atmospheric CO_2 increase. This behavior is known as transient steady state (TSS), since it assumes that the increase in C_{ant} in the ocean occurs with a steady state ocean circulation [*Tanhua et al.*, 2006; *Steinfeldt et al.*, 2009]. *Fajar et al.* [2015] found that, along 7.5°N , the rate of C_{ant} increase agrees with the TSS for deep waters, but it is larger than expected for the thermocline and intermediate waters. The changes along 24.5°N have been estimated between 1992 and 2011 by *Guallart et al.* [2015]. The largest C_{ant} changes occur in thermocline waters, up to $1 \mu\text{mol kg}^{-1} \text{ yr}^{-1}$. The C_{ant} increase rates for deep waters are much smaller, on average less than $0.25 \mu\text{mol kg}^{-1} \text{ yr}^{-1}$, largest in the westernmost margin.

Hernández-Guerra et al. [2014] described the general circulation along 7.5°N and 24.5°N , for the same realizations studied by *Fajar et al.* [2015] and *Guallart et al.* [2015]. According to their study, a three-layer circulation pattern is defined for both sections. Antarctic Bottom Water (AABW), the densest water in the ocean, flows northward in the western side of the sections. Lower and upper North Atlantic Deep Water (INADW and uNADW) fill the deep layer, roughly between 1500 and 4200 m depth, flowing to the south. The circulation in the upper layer differs between both sections. Antarctic Intermediate Water (AAIW) and South Atlantic Central Water (SACW) are found at the 7.5°N section flowing northward. At 24.5°N we find AAIW, Mediterranean Water, and North Atlantic Central Water (NACW). The integrated thermocline mass transport at 24.5°N is northward because of the flow through the Florida Strait; if the Florida Current is not considered, the NACW flows south as a result of the wind stress curl [*Fraille-Nuez and Hernández-Guerra*, 2006]. The differences in mass transport between 1993 and 2010 (1992 and 2011) at 7.5°N (24.5°N) sections were also analyzed by *Hernández-Guerra et al.* [2014]. The most noteworthy changes are listed below. The AMOC, defined as the maximum of the zonally and vertically integrated mass transport from surface downward, is stronger in 1992–1993 than in 2010–2011, the difference being larger in 7.5°N than in 24.5°N . Much of this change results from the northward flow of AAIW, which was more energetic in 1992–1993 than in 2010–2011.

This paper examines the changes in C_{ant} transport across 7.5°N and 24.5°N and what these variations tell us about the C_{ant} budget in the TNA. The C_{ant} transports through the two North Atlantic sections are used to detect changes over nearly two decades and to disentangle the relative contribution of changes in both C_{ant} and velocity fields to the variations in C_{ant} transport. Finally, C_{ant} air-sea flux is inferred from the C_{ant} lateral transports and the C_{ant} storage rates, closing the C_{ant} budget in the TNA.

Table 1. Cruise Information

Cruise	Date	Ship	Chief Scientist	References
7.5°N-1993 CITHER	13/02/1993 to 19/03/1993	<i>L'Atalante</i>	C. Colin (ORSTOM, France)	<i>Arhan et al.</i> [1998]; <i>Oudot et al.</i> 1995
7.5°N-2010 MOC2	5/04/2010 to 16/05/2010	<i>Hespérides</i>	J. L. Pelegrí (Institut de Ciències del Mar, Spain)	<i>Hernández-Guerra et al.</i> [2014]; <i>Rios et al.</i> [2012]
24.5°N-1992	14/07/1992 to 15/08/1992	<i>Hespérides</i>	G. Parrilla (Instituto Español de Oceanografía, Spain)	<i>Lavin et al.</i> 1998; <i>Rosón et al.</i> [2003]
24.5°N-2011	27/01/2011 to 15/03/2011	<i>Sarmiento de Gamboa</i>	A. Hernández-Guerra (Universidad de Las Palmas de Gran Canaria, Spain)	<i>Hernández-Guerra et al.</i> [2014]; <i>Guallart et al.</i> [2015]

2. Data and Methods

2.1. Cruises

The 7.5°N section was first occupied in February–March 1993 by the French R/V *L'Atalante*, as part of the Circulation THERmohaline (CITHER) project [Oudot et al., 1998; Arhan et al., 1998; Lux et al., 2001]. This section contributed to the WOCE (World Ocean Circulation Experiment) Hydrographic Programme under the denomination A6. During this cruise, 84 full-depth hydrographic stations were carried out. Water samples were taken and analyzed for oxygen, nutrients [Oudot et al., 1998], total alkalinity (A_T), and pH, necessary to calculate the total inorganic CO_2 (C_T) [Oudot et al., 1995]. The section was repeated in April–May 2010 on board the R/V *Hespérides*, as part of the MOC2 cruise [San Antolín Plaza et al., 2012; Hernández-Guerra et al., 2014]. During that cruise a total of 59 full-depth hydrographic stations were carried out, also taking water samples for the analysis of oxygen, nutrients, A_T , and pH. Total inorganic CO_2 (C_T) was calculated from A_T and pH measurements. More information about both cruises is presented in Table 1, with the positions of the stations shown in Figure 1.

The 24.5°N section has been occupied several times since 1957, but it was in 1992 when the properties for defining the CO_2 system were first measured. In this work we use data from two cruises along this section, carried out in 1992 and in 2011. During the 1992 cruise, 112 full-depth hydrographic stations were completed, 11 of them in the Florida Straits. Water samples were taken and nutrients, A_T , and pH were measured, and C_T was calculated [Rosón et al., 2003]. That cruise was a contribution to the WOCE hydrographic program under the denomination A5. During the 2011 cruise, under the umbrella of the Malaspina project (www.expedicionmalaspina.es), 167 full-depth hydrographic stations were carried out, 13 of them in the Florida Straits [Hernández-Guerra et al., 2014]. Bottle samples were collected to measure oxygen, nutrients, A_T , and pH, and C_T was calculated [Guallart et al., 2015].

2.2. Methods

2.2.1. C_{ant} Estimations

The concentration of C_{ant} in sea water is not directly measurable since natural and anthropogenic CO_2 are indistinguishable. There are several methods to estimate C_{ant} in the sea water, but all of them belong to

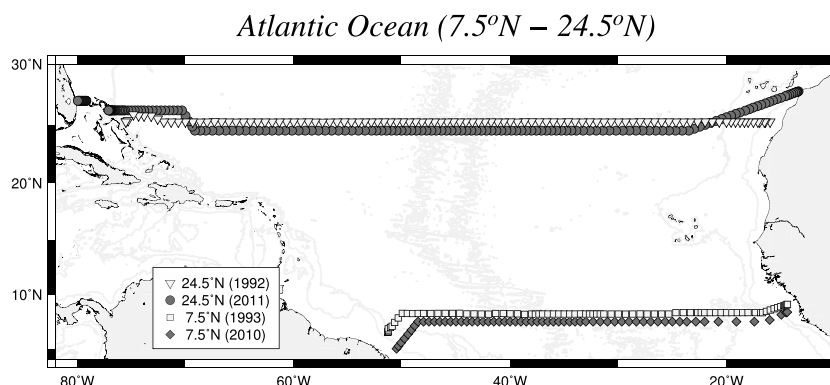


Figure 1. Location of the full-depth hydrographic stations carried out along the 24.5°N (7.5°N) in 1992 and 2011 (1993 and 2010). The 1992 and 1993 cruise tracks are offset 0.5° in latitude for clarity.

Table 2. Definition of the 17 Layers Included in the Inverse Model for Computing the Mass Transports^a

Layer	Lower Interface (γ_n , kg m ⁻³)	Water Masses
1	26.4400	Surface water
2	26.8500	
3	27.1620	SACW/NACW
4	27.3800	
5	27.6200	
6	27.8200	AAIW
7	27.9220	
8	27.9750	uNADW
9	28.0080	
10	28.0440	
11	28.0720	INADW
12	28.0986	
13	28.1100	
14	28.1295	
15	28.1410	AABW
16	28.1540	
17	bottom	

^aThe lower interface limit of each layer and the approximate equivalence with water masses are indicated. The layers in the inverse model were specified as separated by isoneutrals.

the air-sea CO₂ disequilibrium is considered. In particular, the ϕC_T^0 method is characterized by assuming non-constant air-sea CO₂ disequilibrium and using a robust preformed A_T. The TTD method is based on CFC observations. All these methods have strengths and weaknesses with uncertainties ranging from ± 2 to $\pm 9 \mu\text{mol kg}^{-1}$ [see *Khaliwala et al.*, 2013, Table A1]. For an intercomparison between these methods in the Atlantic Ocean the reader is referred to *Vázquez Rodríguez et al.* [2009]. *Guallart et al.* [2015] evaluated the consistence between different methods estimating C_{ant} storage rates at the 24.5°N section; they found a good agreement between the results obtained from four different methods (ϕC_T^0 , TrOCA, ΔC^* , and TTD). In the present work, C_{ant} at both 7.5°N and 24.5°N is obtained using a back-calculation method, specifically the ϕC_T^0 method [Vázquez Rodríguez et al., 2009] where C_{ant} is determined from C_T, A_T, oxygen, nutrients, temperature, and salinity. The uncertainty of this method is $\pm 5.2 \mu\text{mol kg}^{-1}$.

2.2.2. Transport of C_{ant}

The total transport of any property across a transoceanic section is quantified as

$$T_{\text{prop}} = \int_{\text{east}}^{\text{west}} \int_{\text{bottom}}^{\text{surface}} \rho [\text{prop}] v \, dx dz \quad (1)$$

where ρ , [prop], and v stand for in situ density, property concentration per unit mass, and velocity perpendicular to the section, respectively. We obtain C_{ant} transport (kmol s⁻¹) taking [prop] as C_{ant} concentration ($\mu\text{mol kg}^{-1}$).

The absolute velocity components perpendicular to the 7.5°N and 24.5°N sections were estimated using an inverse box model, combining data from both sections. The inverse model was defined by 17 neutral surfaces (γ_n , Table 2). These surfaces (hereafter simply neutral surfaces or isoneutrals) essentially represent a potential density surface (isopycnal) with a continuous changing reference level. Isonetrals increase smoothly with depth avoiding the discontinuities that arise when computing the potential densities relative to a limited number of reference levels [Jackett and McDougall, 1997]. The absolute velocity is computed as the sum of a reference velocity at some properly specified reference level plus a relative velocity contribution, calculated from the density field under the assumption of geostrophic balance. The inverse model includes surface Ekman transport and, after imposing several constraints for particular ranges of depths and longitudes, solves for the reference-level velocities and the vertical velocities between adjacent isoneutral layers that best satisfy mass conservation for each layer and the whole water column. For more details about the inverse model the reader is referred to *Hernández-Guerra et al.* [2014].

Following the general circulation pattern across 7.5°N and 24.5°N sections exposed in section 1, the transport of C_{ant} is analyzed by layers. Three main layers are defined. The upper layer extends from the surface down to $\gamma_n = 27.922 \text{ kg m}^{-3}$; it contains SACW, NACW, and AAIW. The deep layer goes from $\gamma_n = 27.922 \text{ kg m}^{-3}$ down

Table 3. C_{ant} Change Rates Estimated for Each Water Mass at 7.5°N and 24.5°N (Referenced to Year 2001)

7.5°N Section			24.5°N Section		
Water Mass	Density Limits	C_{ant} Rate ($\mu\text{mol kg}^{-1} \text{yr}^{-1}$)	Water Mass	Density Limits	C_{ant} Rate ($\mu\text{mol kg}^{-1} \text{yr}^{-1}$)
SACW	$\sigma_0 < 26.5$	0.766 ± 0.097	uNACW	$\sigma_0 < 26.7$	0.989 ± 0.066
SACW	$26.5 < \sigma_0 < 27.1$	0.750 ± 0.091	INACW	$26.7 < \sigma_0 < 27.2$	0.438 ± 0.063
AAIW	$27.1 < \sigma_0 < 27.5$	0.480 ± 0.062	AAIW	$27.2 < \sigma_0 < 27.6$	0.251 ± 0.054
uNADW	$\sigma_0 > 27.5$ and $\sigma_2 < 37$	0.143 ± 0.005	uNADW	$\sigma_0 > 27.6$ and $\sigma_2 < 37$	0.198 ± 0.010
INADW	$\sigma_2 > 37$ and $\sigma_4 < 45.9$	0.119 ± 0.005	INADW	$\sigma_2 > 37, \sigma_4 < 45.9$	0.140 ± 0.010
AABW	$\sigma_4 > 45.9$	0.127 ± 0.034	AABW	$\sigma_4 > 45.9$	0.160 ± 0.017

to $\gamma_n = 28.141 \text{ kg m}^{-3}$; it holds uNADW and INADW. The bottom layer lies between $\gamma_n = 28.141 \text{ kg m}^{-3}$ and the sea bottom, comprising AABW.

The error of C_{ant} transport is computed as the sum of errors due to both the mass transport and the C_{ant} uncertainties. The former is calculated from the covariance matrix of errors for mass transport, as obtained from the inverse model [Hernández-Guerra *et al.*, 2014]. To estimate the C_{ant} transport error associated to the C_{ant} uncertainty, C_{ant} transports are computed from 100 random perturbed C_{ant} data (zero mean and standard deviation of $5.2 \mu\text{mol kg}^{-1}$); the uncertainty is determined by the standard error of the 100 perturbations.

2.2.3. Storage Rate of C_{ant}

The second part of this paper explores the C_{ant} budget in the TNA. The budget of C_{ant} in an oceanic box is the balance between three terms: C_{ant} laterally advected, accumulation of C_{ant} , and C_{ant} fluxes through the air-sea interface. We define our TNA region as the volume of water contained between 7.5°N and 24.5°N and the American and African continents, including the Caribbean Sea. The lateral advection of C_{ant} to the TNA region comes from the C_{ant} transports across the 7.5°N and 24.5°N sections. The air-sea flux of C_{ant} is not directly measurable, being inferred from the other two components of the C_{ant} budget. The calculation of the C_{ant} storage rates is more laborious, being estimated from the rates of increase of C_{ant} along the 7.5°N and 24.5°N sections (Table 3), as follows. Fajar *et al.* [2015] estimated the C_{ant} increase rates at 7.5°N as the difference in C_{ant} concentration between 1993 and 2010 divided by the elapsed time and also provided uncertainty values. Guallart *et al.* [2015] obtained the C_{ant} increase rates through a linear regression of data from five occupations of the 24.5°N section, from 1992 to 2011, with the standard deviations providing a measure of the uncertainties. The C_{ant} increase rates for the whole TNA are then computed for each water mass through a weighted average of the northern and southern contributions; specifically, we assume the 7.5°N section to characterize the North Equatorial Current region (reaching till 18°N or 66% of the TNA area) and the 24.5°N sections to represent the remaining area (between 18°N and 24.5°N or 34% of the TNA area). This partition was tested using gridded products of C_{ant} storage and outputs of ocean biogeochemical models [Khatiwala *et al.*, 2009, 2013] giving biases lower than 2%, negligible compared with the uncertainties for the C_{ant} increase rates. Finally, the storage rate of C_{ant} and its uncertainty are calculated for each water mass within the whole TNA region (Table 4). This is done multiplying the C_{ant} increase rate, and its uncertainty, by the corresponding water mass volume. In order to compute these volumes, we use the temperature and salinity data from the World Ocean Atlas 2009 (WOA09) [Locarnini *et al.*, 2010; Antonov *et al.*, 2010] so as to calculate the density-depth fields. The thicknesses of each water mass are estimated for every WOA09 grid point (1° latitude-longitude), after defining the water masses from properly defined potential density intervals (Table 4), and the total volume of each water mass in the TNA region is the integration over all grid points. The error of the volume determination is less than 1%, much less than the uncertainties for the C_{ant} concentration rate (~5–10%).

The C_{ant} budget is examined for the same three layers used for calculating C_{ant} transports. However, we define the main layers in the TNA region by γ_n surfaces, while Fajar *et al.* [2015] and Guallart *et al.* [2015] defined their water masses in terms of isopycnal. Because of this, there is a small mismatch in the lower limit of the AAIW, located within the upper layer. The AAIW lower limit defined by Fajar *et al.* [2015] and Guallart *et al.* [2015] is $\sigma_0 \cong 27.55 \text{ kg m}^{-3}$, while in the isoneutral approximation it is $\gamma_n \cong 27.82 \text{ kg m}^{-3}$

Table 4. Limits, Volumes, C_{ant} Increase Rates, and C_{ant} Storage Rates Computed for Each Water Mass and For the Three Main Layers Defined in Our TNA Region (Referenced to Year 2001)^a

Water Mass or Layer	Limits (kg m ⁻³)	Volume (10 ¹⁵ m ³)	C_{ant} Rate (μmol kg ⁻¹ yr ⁻¹)	C_{ant} Storage Rate for 2001 (Pg C yr ⁻¹)	C_{ant} Storage Rate for 1992 (Pg C yr ⁻¹)	C_{ant} Storage Rate for 2010 (Pg C yr ⁻¹)
SACW/uNACW	$\sigma_0 < 26.6$	3.03	0.877 ± 0.118	0.033 ± 0.004	0.028 ± 0.004	0.038 ± 0.004
SACW/INACW	26.6 < σ_0 < 27.15	4.04	0.594 ± 0.111	0.030 ± 0.006	0.026 ± 0.006	0.034 ± 0.006
AAIW	27.15 < σ_0 < 27.55	5.58	0.365 ± 0.082	0.025 ± 0.006	0.022 ± 0.006	0.029 ± 0.006
AAIW-uNADW ^b	27.55 < σ_0 < 27.70	3.31	0.171 ± 0.028	0.007 ± 0.000	0.006 ± 0.000	0.008 ± 0.000
uNADW	$\sigma_0 > 27.70, \sigma_2 < 37$	14.7	0.171 ± 0.028	0.031 ± 0.003	0.027 ± 0.003	0.036 ± 0.003
INADW	$\sigma_2 < 37, \sigma_4 < 45.9$	18.9	0.129 ± 0.028	0.030 ± 0.003	0.026 ± 0.003	0.035 ± 0.003
AABW	$\sigma_4 > 45.9$	1.71	0.143 ± 0.040	0.003 ± 0.000	0.00 ± 0.000	0.003 ± 0.000
Upper layer	$Y_n < 27.922$	15.96	0.482 ± 0.046	0.095 ± 0.009	0.082 ± 0.009	0.110 ± 0.009
Intermediate layer	27.922 < Y_n < 28.141	33.6	0.147 ± 0.019	0.061 ± 0.008	0.052 ± 0.008	0.071 ± 0.008
Deep layer	28.141 < Y_n	1.71	0.143 ± 0.040	0.003 ± 0.001	0.003 ± 0.001	0.003 ± 0.001
Total		51.3	0.251 ± 0.019	0.159 ± 0.012	0.137 ± 0.012	0.185 ± 0.012

^aThe C_{ant} storage rates referenced to years 1992 and 2010 were deduced from the C_{ant} storage rate for 2001 values using the TSS hypothesis, as explained in the text (equation (2)). 1 Pg C yr⁻¹ = 2642 kmol s⁻¹.

^bThe 27.55 < σ_0 < 27.70 kg m⁻³ water has been separated from AAIW and uNADW because of a small mismatch in the AAIW defined by *Fajar et al.* [2015] and *Guallart et al.* [2015] and our upper layer definition.

[*Macdonald* 1995; *Ganachaud*, 1999] which, for the Atlantic Ocean, corresponds to $\sigma_0 \cong 27.70$ kg m⁻³. Hence, *Fajar et al.* [2015] and *Guallart et al.* [2015] considered 27.55 < σ_0 < 27.70 kg m⁻³ to be part of uNADW, while for the transport calculations it would be part of the upper layer. In order to solve this inconsistency, we proceed as follows: (i) calculate the volume of TNA with 27.55 < σ_0 < 27.70 kg m⁻³, (ii) associate the uNADW C_{ant} rate to this water volume, but (iii) include the corresponding accumulation of C_{ant} in the upper layer of the TNA. Table 4 displays the limits, volumes, and C_{ant} mean rates referenced to year 2001 and the corresponding C_{ant} storage rates for each water mass and each layer within the TNA. Finally, the C_{ant} storage rates are rescaled to 1993 and 2010 following the TSS hypothesis [*Tanhua et al.*, 2006; *Steinfeldt et al.*, 2009], according to the expression

$$T_{\text{Cant}}^{\text{year2}} = T_{\text{Cant}}^{\text{year1}} (1 + 0.0169)^{\text{year2} - \text{year1}} \quad (2)$$

where, in our case, year1 is 2001 and year2 is either 1993 or 2010.

3. Results

3.1. Anthropogenic CO₂ Distribution in the Two Repeated 7.5°N and 24.5°N Atlantic Sections

Figure 2 shows the C_{ant} distribution of the two repetitions along 7.5°N, in 1993 and 2010, as well as along 24.5°N, in 1992 and 2011. In both sections and years, the highest C_{ant} concentrations correspond to the surface waters as a consequence of their direct contact with the atmosphere, with C_{ant} generally decreasing with increasing depth. Regarding the differences between both realizations (elapsed 17/19 years in 7.5°N/24.5°N), the largest increase corresponds to the thermocline waters. Nevertheless, the anthropogenic signal is also detected in NADW (27.922 kg m⁻³ < Y_n < 28.141 kg m⁻³). Along the 7.5°N section, the eastward displacement of NADW is related to a tongue of C_{ant} -enriched water, larger in 2010 than in 1993, located near $Y_n = 27.922$ kg m⁻³. Along the 24.5°N section, the arrival of C_{ant} -enriched NADW is also detected in the western basin, associated with a relative maximum of C_{ant} concentration (> 20 μmol kg⁻¹ in 2011 on $Y_n = 27.922$ kg m⁻³) even reaching the INADW (C_{ant} concentration > 10 μmol kg⁻¹ in 2011 on $Y_n > 28.072$ kg m⁻³).

Figure 3 displays the section mean profiles of C_{ant} averaged on isoneutral surfaces. The largest (and statistically significant) C_{ant} temporal increase along the 7.5°N section (between 1993 and 2010) is detected within the SACW stratum (some 12 μmol kg⁻¹) followed by the AAIW stratum (about 5 μmol kg⁻¹) (Figure 3a). Deeper in the water column (NADW and AABW), the 1993 and 2010 section mean profiles are not statistically different. In the 24.5°N section (Figure 3b) the behavior is similar to that observed at 7.5°N, with the C_{ant} increasing significantly in the NACW (13 μmol kg⁻¹) and AAIW (6 μmol kg⁻¹) strata. The C_{ant} increase in the uNADW is also statistically significant, but this is not true for the INADW and AABW.

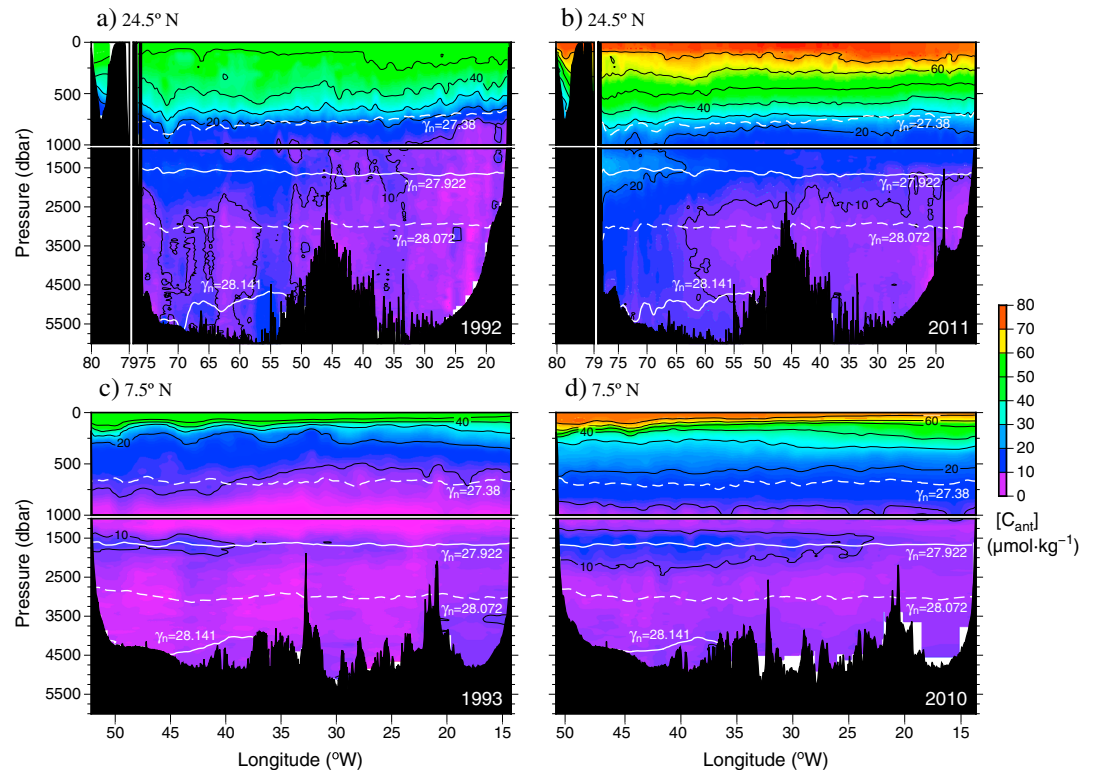


Figure 2. Vertical section of C_{ant} ($\mu\text{mol kg}^{-1}$) along 24.5°N in (a) 1992 and (b) 2011 and along 7.5°N in (c) 1993 and (d) 2010. White lines point out the position of isoneutral surfaces (γ_n) delimiting the water masses. Continuous white lines split the section into the upper, deep, and bottom layers analyzed in this work, corresponding also to limits between water masses.

A comparison of the C_{ant} concentration profiles at 24.5°N and 7.5°N (Figures 3c and 3d) shows that they are statistically different in most of the whole water column, with concentrations always larger in 24.5°N than in 7.5°N. The largest difference between both mean profiles is detected at the central water (SACW and NACW) level. This difference is likely related to the different times elapsed for the subpolar/subantarctic components of NACW/SACW ($26.85 < \gamma_n < 27.38$) to reach the 24.5°N and 7.5°N sections from their water formation areas. The subantarctic component of SACW is formed south of 45°S, in the Subantarctic Front [Stramma and Schott, 1999], while the subpolar component of the NACW is formed in the subpolar North Atlantic (45–52°N), where it is ventilated relatively fast [McCartney and Talley, 1982]. Hence, the SACW at 7.5°N shows less C_{ant} than the NACW at 24.5°N. Notice that surface waters do not show a marked spatial gradient because all thermocline waters of subtropical and tropical areas are locally ventilated in time periods of only a few years, incorporating C_{ant} from the atmosphere at a very similar rate.

3.2. Transport of Anthropogenic CO₂ Across Two Tropical North Atlantic Sections

3.2.1. The 7.5°N Section

This is the first time that C_{ant} transport across the 7.5°N section is investigated using in situ data. The meridional transport of C_{ant} across the 7.5°N section is northward and increases from $315 \pm 47 \text{ kmol s}^{-1}$ in 1993 to $493 \pm 51 \text{ kmol s}^{-1}$ in 2010. The increase in the C_{ant} transport may be explained in terms of both circulation and/or C_{ant} changes. Next, we elucidate on the contribution of both factors in the observed C_{ant} transport changes.

The different patterns of mass transport across 7.5°N in 1993 and 2010 were studied in detail by Hernández-Guerra *et al.* [2014]. They found the AMOC to be stronger in 1993 than in 2010, $29.2 \pm 1.7 \times 10^9 \text{ kg s}^{-1}$ as compared with $16.9 \pm 1.5 \times 10^9 \text{ kg s}^{-1}$. An important part of this decrease was related to a change in the northward transport of AAIW, which was more intense in 1993 than in 2010; this intensification of the northward AAIW transport is balanced by a larger southward transport of INADW in 1993 than in 2010.

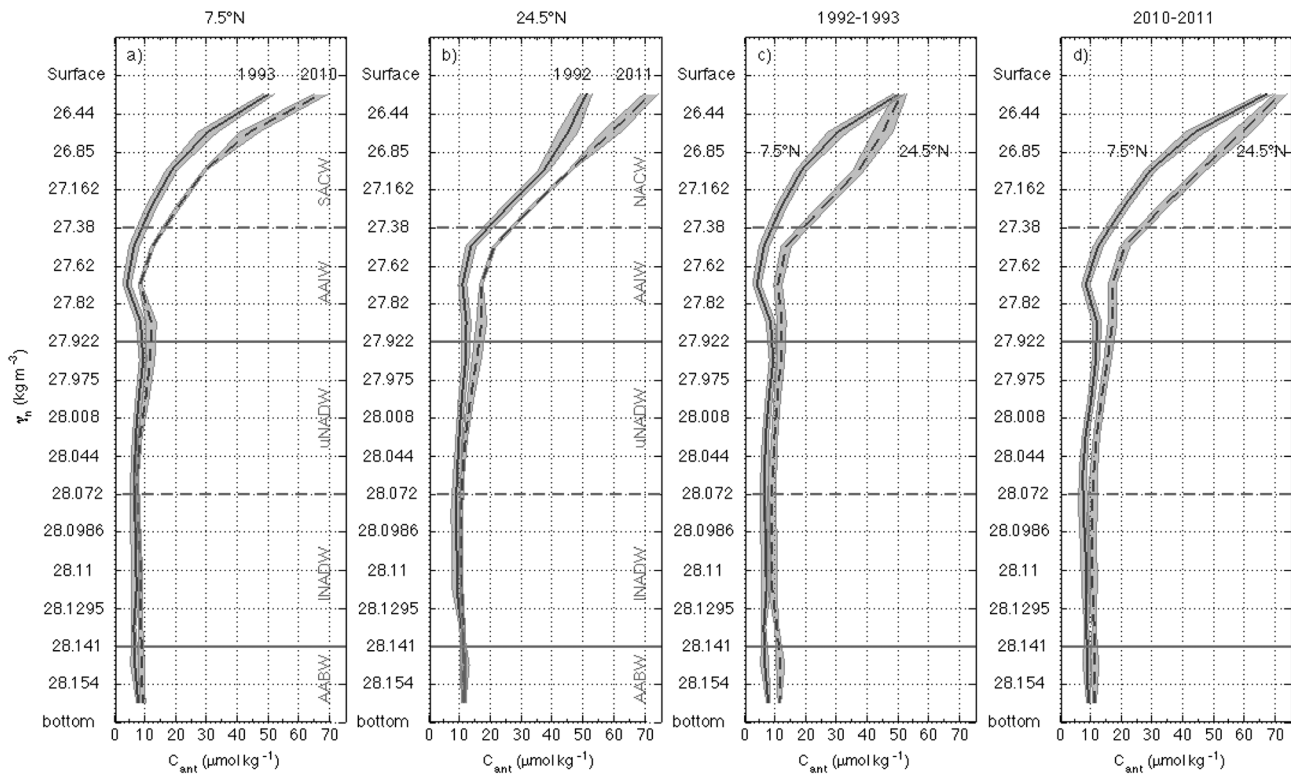


Figure 3. Section mean profiles of C_{ant} averaged on isoneutrals surfaces (γ_n) showing the time increase at (a) 7.5°N and (b) 24.5°N and (c and d) the latitudinal differences between 7.5°N and 24.5°N. Shaded contours show the standard deviation of the section mean values. Grey lines stand for the position of water masses in the water column. Continuous grey lines are drawn to visualize the three main layers: upper, deep, and bottom. SACW: South Atlantic Central Water; NACW: North Atlantic Central Water; AAIW: Antarctic Intermediate Water; uNADW: upper North Atlantic Deep Water; INACW: lower North Atlantic Deep Water; AABW: Antarctic Bottom Water.

The principal changes in mass transport found by *Hernández-Guerra et al.* [2014] can also be observed in Figure 4a.

Despite that the AMOC mass transport across 7.5°N decreased between 1993 and 2010, the C_{ant} transport increased from $315 \pm 47 \text{ kmol s}^{-1}$ to $493 \pm 51 \text{ kmol s}^{-1}$. This increase is explained both by the weaker 2010 southward C_{ant} transport in the deep layer and by the stronger 2010 northward C_{ant} transport in the upper layer. Table 5 shows the zonally integrated mass transport in the upper, deep, and bottom layers in 1993 and 2010. The decrease in the northward (southward) mass transport in the upper (deep) layer is $8.9 \times 10^9 \text{ kg s}^{-1}$ ($9.0 \times 10^9 \text{ kg s}^{-1}$) which means an average reduction of about 35%. In contrast, the upper layer experienced a 21% increase in northward C_{ant} transport, while the deep layer underwent a 33% decrease in southward C_{ant} transport (Table 5). The large decrease in deep mass transport is the cause of the C_{ant} transport decrease in the deep layer. However, the principal factor controlling the changes in C_{ant} transport by the upper layer is the increase in C_{ant} within thermocline waters, much more relevant than the decrease in mass transport. The minor relevance of the mass transport change is because it was mainly affecting AAIW, a water mass with moderate C_{ant} concentration.

Another important factor controlling the C_{ant} transport across 7.5°N is the change in the horizontal circulation pattern. Figure 5 shows the mass and C_{ant} transports in the upper, deep, and bottom layers during 1993 and 2010. First, despite the similar mass transports in the eastern margin of the upper layer (Figure 5a), the C_{ant} transport was slightly larger in 2010 than in 1993 (Figure 5d) as a result of the relatively large C_{ant} increase in the eastern margin [*Fajar et al.*, 2015]. Second, the large difference in mass transport at 30°W–35°W is not observed in the C_{ant} transport; this is caused by both the relatively large C_{ant} increase undergone by the SACW at this location [*Fajar et al.*, 2015] and the weakening of the AAIW northward transport which, because of its relatively low C_{ant} concentration, does not imply an important change in the C_{ant} transport.

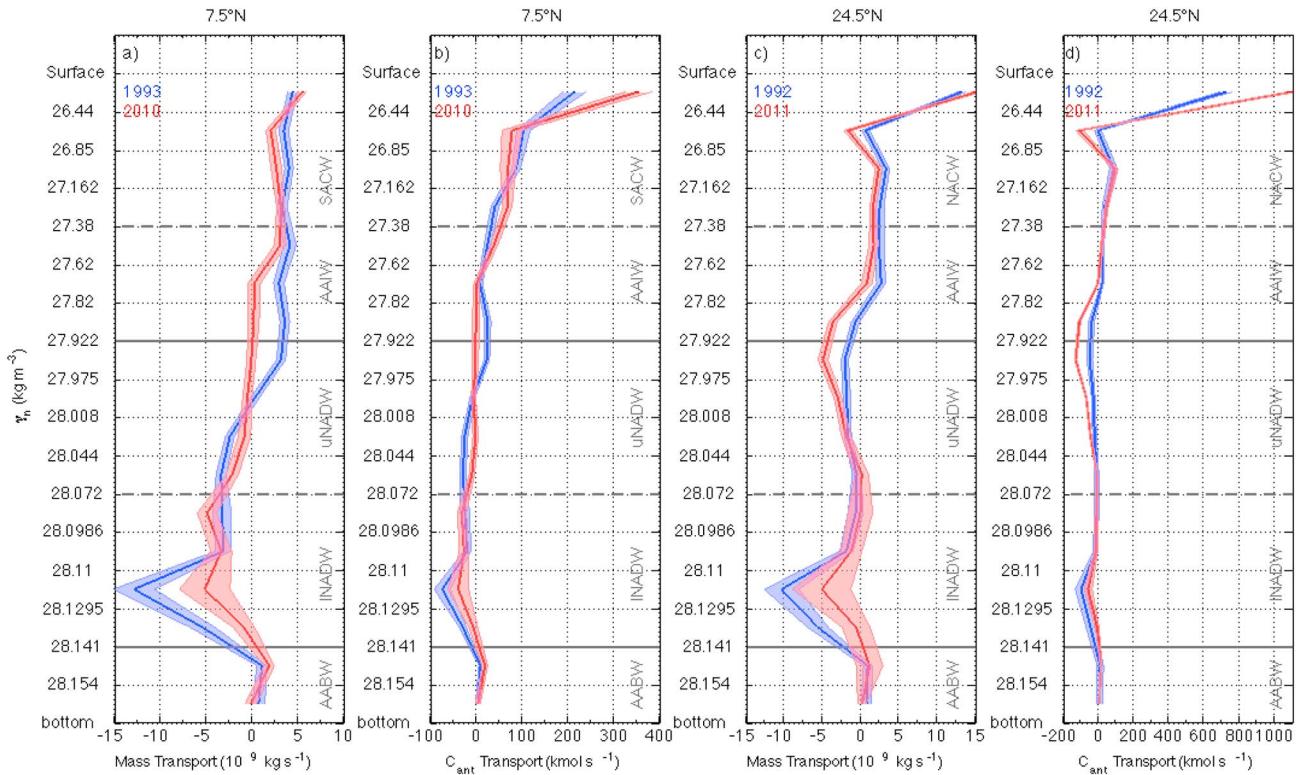


Figure 4. Zonally integrated transport of mass and C_{ant} (a and b) across the 7.5°N section and (c and d) across the 24.5°N section. Positive (negative) values point out northward (southward) transport. Red (blue) lines stand for the older (more recent) periods. Shaded contours represent the error of the zonally integrated transport of mass and C_{ant} at each isoneutral surface. Grey lines stand for the positioning of water masses in the water column. Continuous grey lines are drawn to visualize the three main layers: upper, deep, and bottom. Acronyms are the same as in Figure 3.

The deep layer can be separated into two regions with different dynamics (Figure 5b). East of 35°W, the 1993 mass transport is basically negligible or slightly negative, while the 2010 one shows a weak northward transport. West of 35°W, there is substantial variability in both realizations, of weaker amplitude and shorter spatial scale during 2010 than in 1993. The C_{ant} changes in uNADW and INADW are significant but very small [Fajar et al., 2015]; therefore, the changes in C_{ant} transport basically mirror those in mass transport (Figures 5b and 5e). The zonally integrated C_{ant} (mass) transport in the deep layer is weaker in 2010 than in 1993; i.e., $-128 \pm 34 \text{ kmol s}^{-1}$ ($-18.5 \pm 3.6 \times 10^9 \text{ kg s}^{-1}$) as compared with $-192 \pm 32 \text{ kmol s}^{-1}$ ($-27.5 \pm 3.0 \times 10^9 \text{ kg s}^{-1}$). Therefore, despite a slight C_{ant} increase in the NADW [Fajar et al., 2015], the C_{ant} transport decreases as a result of the reduced southward mass transport. The latter is partially explained by the regional recirculation east of 35°W observed in 2010 and not in 1993.

Finally, no statistically significant differences between 1993 and 2010 have been detected in the mass and C_{ant} transports in the bottom layer between (Figures 5c and 5f).

Table 5. Mass and C_{ant} Transport Across 7.5°N and 24.5°N Integrated for the Three Main Layers

Layers	7.5°N Section				24.5°N Section			
	Mass Transport (10^9 kg s^{-1})		C_{ant} Transport (kmol s^{-1})		Mass Transport (10^9 kg s^{-1})		C_{ant} Transport (kmol s^{-1})	
	1993	2010	1993	2010	1992	2011	1992	2011
Upper $\gamma_n < 27.922$	25 ± 1.5	16.1 ± 1.5	495 ± 42	600 ± 49	23.1 ± 1.9	15.6 ± 1.7	822 ± 45	1012 ± 49
Deep $27.922 > \gamma_n < 28.141$	-27.5 ± 3.0	-18.5 ± 3.6	-192 ± 32	-128 ± 34	-25.4 ± 5.1	-17.5 ± 4.9	-304 ± 51	-362 ± 55
Bottom $\gamma_n > 28.141$	1.6 ± 0.9	1.5 ± 0.8	11 ± 9	27 ± 11	1.4 ± 1.8	1.1 ± 1.8	12 ± 23	12 ± 20
Total	-0.9	-0.9	315 ± 47	493 ± 51	-0.9	-0.8	530 ± 46	662 ± 49

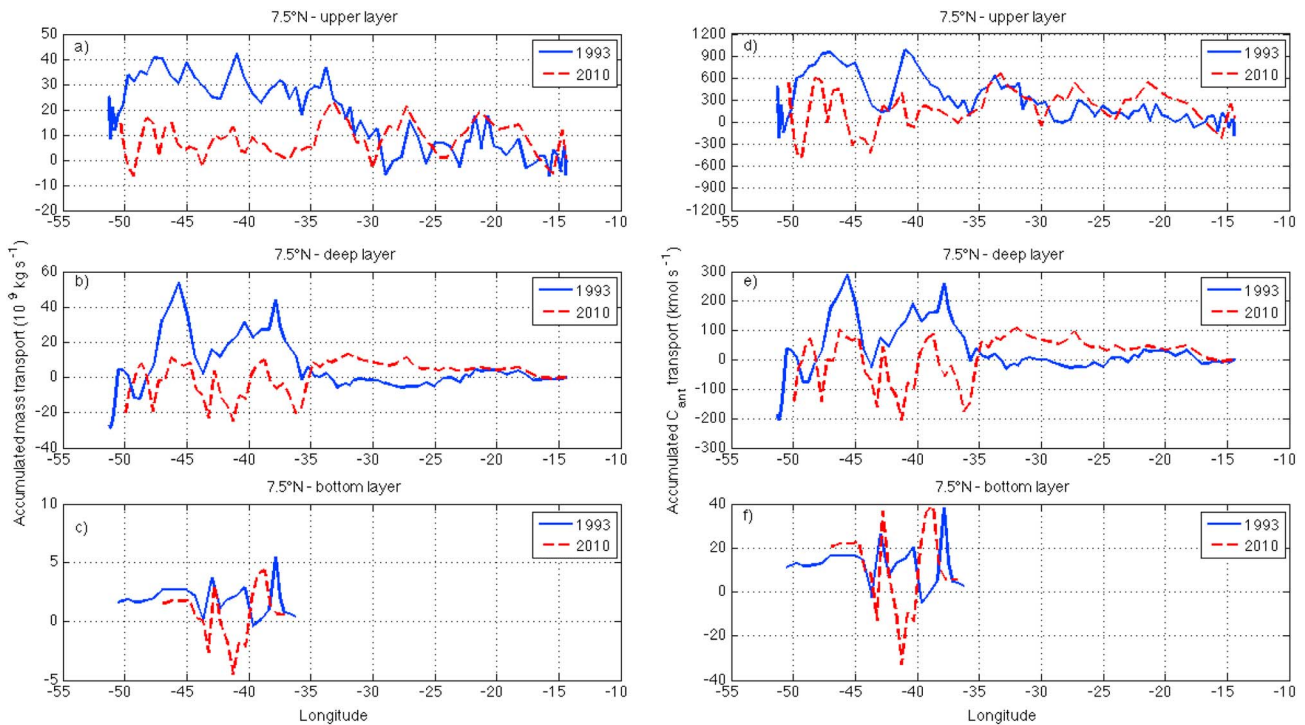


Figure 5. Westward accumulated transport of (a, b, and c) mass and (d, e, and f) C_{ant} in the upper (Figures 5a and 5d), deep (Figures 5b and 5e), and bottom (Figures 5c and 5f) layers along 7.5°N.

3.2.2. The 24.5°N Section

The net mass transport across the 24.5°N section is around $-1 \times 10^9 \text{ kg s}^{-1}$ southward, including the flow in the Bering Strait [Hernández-Guerra *et al.*, 2014; Macdonald *et al.*, 2003; Lavin *et al.*, 1998]. However, since the C_{ant} concentration is larger in the upper than in the interior ocean, the net C_{ant} transport across this section is northward. The meridional transport of C_{ant} across the 24.5°N section increases from $530 \pm 46 \text{ kmol s}^{-1}$ in 1992 to $662 \pm 49 \text{ kmol s}^{-1}$ in 2011. If the Florida Strait is excluded of the analysis, the meridional C_{ant} transport across the 24.5°N section is southward, increasing from $-884 \pm 71 \text{ kmol s}^{-1}$ in 1992 to $-1334 \pm 75 \text{ kmol s}^{-1}$ in 2011. Finally, the C_{ant} transported by the northward Florida Current also increases from $1414 \pm 11 \text{ kmol s}^{-1}$ in 1992 to $1996 \pm 17 \text{ kmol s}^{-1}$ in 2011.

The 1992–2011 differences of mass transport across this section were described by Hernández-Guerra *et al.* [2014]. They observed a decrease of the AMOC intensity from $24.7 \pm 1.7 \times 10^9 \text{ kg s}^{-1}$ in 1992 to $20.1 \pm 1.4 \times 10^9 \text{ kg s}^{-1}$ in 2011. Most of the change in AMOC was associated to the change in the northward transport of AAIW. Figure 4c shows the changes in the mass transport between 1992 and 2011. A decrease in the northward transport of AAIW is observed, even with a flow reversal in the lower part of the AAIW stratum (Figure 4c). Hernández-Guerra *et al.* [2014] also found an increase in the southward transport of uNADW, which was partly compensated by a decrease in the southward transport of INADW (Figure 4c).

As shown by the integrated transports in the three main layers (Table 5), the northward (southward) mass transport in the upper (deep) layer is more intense in 1992 than in 2011. However, we find an increase in the northward (southward) C_{ant} transport in the upper (deep) layer from 1992 to 2011. The increase in the northward C_{ant} transport in the upper layer is basically due to the C_{ant} increase. This C_{ant} increase, as evidenced by Figure 3b, has been reported by Guallart *et al.* [2015]. The increase of the southward C_{ant} transport in the deep layer is explained by changes in the circulation pattern: in 2011 the southward transport of INADW was reduced as compared with 1992 and partially compensated by a larger southward transport of uNADW (Figure 4c). This means that the southward flow in 2011 is shallower and more enriched in C_{ant} than in 1992.

The influence of the zonal distributions in meridional velocity and C_{ant} on the transport of this property across the 24.5°N is also investigated here. In the upper layer, there is a decrease in the zonally integrated mass

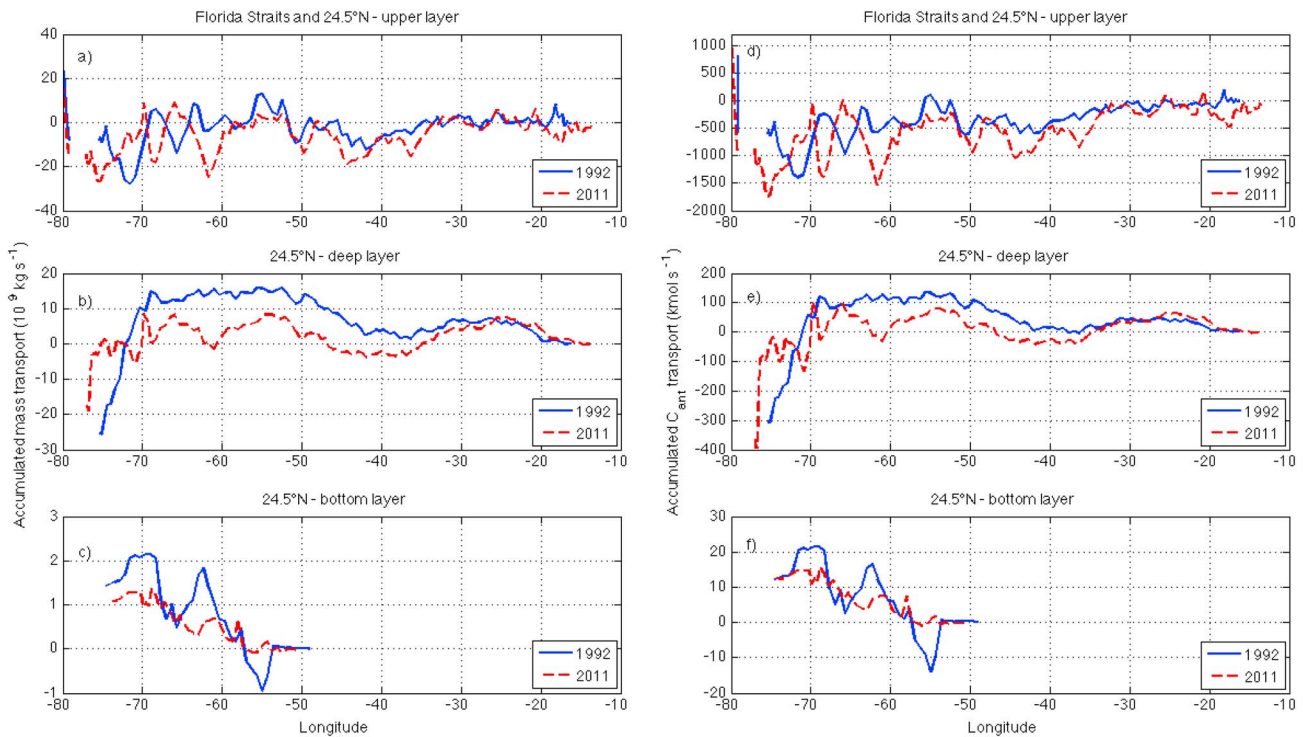


Figure 6. As for Figure 5 but along 24.5°N.

transport from $23.1 \pm 1.9 \times 10^9 \text{ kg s}^{-1}$ in 1992 to $15.6 \pm 1.7 \times 10^9 \text{ kg s}^{-1}$ in 2011 (Table 5). Figure 6 displays the westward accumulated mass and C_{ant} transports in the upper, deep, and bottom layers. During both cruises, the upper layer is characterized by substantial mesoscale circulation along the whole section, and the transport by the Florida Current is rather similar ($31.0 \pm 0.2 \times 10^9 \text{ kg s}^{-1}$ and $31.8 \pm 0.3 \times 10^9 \text{ kg s}^{-1}$ in 1992 and 2011, respectively). Therefore, the decrease from 1992 to 2011 in the northward mass transport is mainly due to the southward transport along the section. The westward accumulated mass transport, excluding the Florida Current from the zonal integration, is $-7.9 \pm 1.7 \times 10^9 \text{ kg s}^{-1}$ and $-16.2 \pm 1.4 \times 10^9 \text{ kg s}^{-1}$ in 1992 and 2011, respectively. As a consequence, the zonally integrated mass transport (including the Florida Current) is smaller in 2011 than in 1992. Regarding the C_{ant} transport in the upper layer (Figure 6d), the major changes occur in the western basin, west of 60°W, reflecting the relevance of mesoscale variability. The westward accumulated transport of C_{ant} up to the Florida Straits is larger in 2011 ($-984 \pm 47 \text{ kmol s}^{-1}$) than in 1992 (-592 ± 43), not only because of the stronger southward transport observed in 2011 but also as a result of the higher C_{ant} concentration in the upper layers in 2011 than in 1992 [Guallart *et al.*, 2015]. In spite of this 2011 increase in the southward C_{ant} transport, the zonally integrated C_{ant} transport (including the Florida Straits) is northward, which is larger in 2011 ($1012 \pm 49 \text{ kmol s}^{-1}$) than in 1992 ($822 \pm 45 \text{ kmol s}^{-1}$). This is because of the large increase in C_{ant} transported by the Florida Current, $1414 \pm 11 \text{ kmol s}^{-1}$ and $1996 \pm 17 \text{ kmol s}^{-1}$ in 1992 and 2011, respectively. The mass transport variability of the Florida Current is rather stable; therefore, the increase in C_{ant} transport associated to the Florida Current is chiefly due to the C_{ant} increase in the Florida Strait waters [Guallart *et al.*, 2015].

There are some differences between the two 24.5°N repetitions in the horizontal circulation of the deep layer. The most remarkable differences are the 2011 moderately stronger southward mass transport between 30 and 40°W (Figure 6b) and the 1992 stronger southward mass transport in the western boundary (Figure 6b) associated to the deep western boundary current (DWBC). The southward C_{ant} transport between 30 and 40°W (Figure 6e) is also stronger in 2011 than in 1992. However, contrary to the mass transport, the C_{ant} transport associated to the DWBC is stronger in 2011 than in 1992; this is because of the different main contributor to the southward mass transport, the uNADW in 2011 and the INADW in

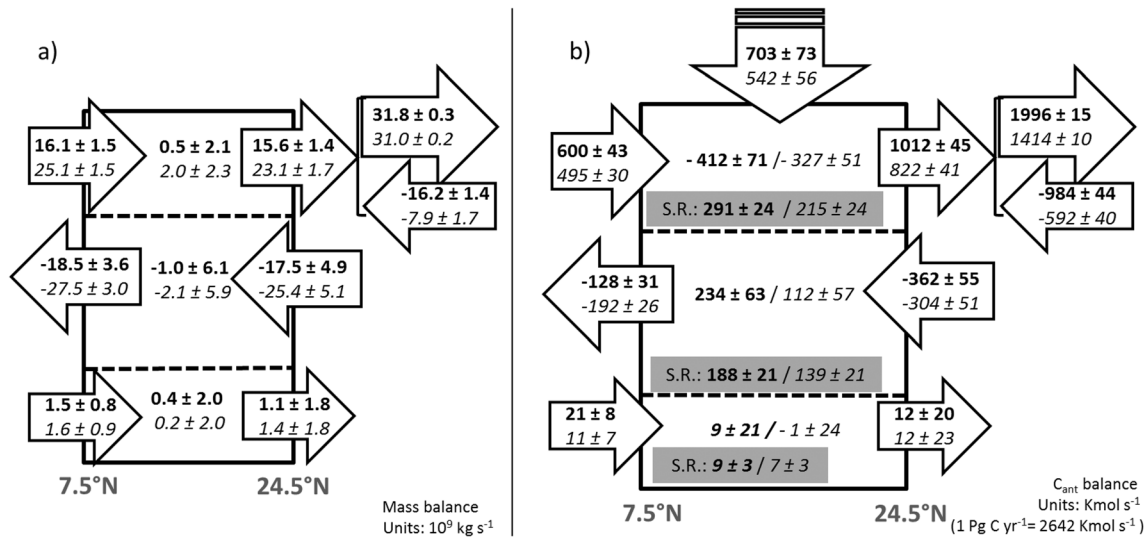


Figure 7. (a) Schematic of mass balance in the three layers defined for the TNA, during both 2010–2011 (bold font) and 1992–1993 (italic font) (10^9 kg s^{-1}). The TNA region is the volume of water contained between 7.5°N and 24.5°N and the American and African continents, including the Caribbean Sea. South (North) is on the left (right) side of the box. Discontinuous lines inside the box split the water column into three main layers: upper (top), deep (middle), and bottom (bottom). Horizontal arrows stand for the northward (positive) and southward (negative) transport. In the case of the transport at the 24.5°N upper layer, three different arrows are shown: the left arrow corresponds to the total transport across the 24.5°N upper layer, which is equal to the sum of the transport by the Florida current (upper right arrow) and the accumulated transport east of the Florida Straits (lower right arrow). The numbers inside each layer are the net input (positive values) or output (negative values). (b) Schematic of the C_{ant} budget in the TNA, during both 2010–2011 (bold font) and 1992–1993 (italic font) (kmol s^{-1}). Notation is the same as in Figure 7a; additionally, grey boxes show C_{ant} storage rates which, for the bottom and deep layers, are to be compared with the net input; for the upper layer the balance is closed through the air-sea C_{ant} transfer (vertical arrow).

1992 (Figure 4c), with the C_{ant} concentration and the C_{ant} rate being higher within the uNADW than within the INADW (Figure 3b).

In the bottom layer the mass and C_{ant} transports in 1992 and 2011 are not statistically different.

3.3. Anthropogenic CO_2 Budget in the Tropical North Atlantic

The repetition of the 7.5°N and 24.5°N sections allows not only to quantify the changes in C_{ant} transport between two states separated by almost two decades but also to evaluate, for the first time with the help of in situ data, the C_{ant} budget in the TNA. Consider first the situation during 2010–2011 as the first step we examine if mass is conserved within the TNA. The inverse model used for computing the mass transport across 7.5°N and 24.5°N also calculates the diapycnal transports between different layers [Hernández-Guerra *et al.*, 2014]. Diapycnal transport is statistically different from zero only between layers within the uNADW; i.e., no significant diapycnal velocities take place between the three main layers we have considered (upper, deep, and bottom). Figure 7 shows the balance of mass and C_{ant} within these three layers, with the box representing the volume of water contained within the TNA region. The mass conservation is satisfied in each individual layer (Figure 7a) as well as for the whole volume of water; hence, it allows evaluating the C_{ant} budget for each layer and for the whole volume of water.

The net input/output of C_{ant} into the TNA is examined for each layer. For the bottom layer, it is not statistically different from zero (Figure 7b). For the deep layer, there is net C_{ant} input of $234 \pm 65 \text{ kmol s}^{-1}$ (Figure 7b) or $0.09 \pm 0.02 \text{ Pg C yr}^{-1}$. The DWBC causes an important injection of relatively rich C_{ant} NADW across 24.5°N into the TNA (Figures 6b and 6e). However, this flux of C_{ant} is not so intense across the 7.5°N section because of the recirculation of NADW, taking place near the western margin (Figures 5b and 5e). The accumulation of C_{ant} in the deep layer due to the lateral transport is estimated here neglecting vertical diffusion between layers. The storage rate of C_{ant} is calculated to elucidate whether the accumulation of C_{ant} in the deep layer is only accounted by lateral advection. Our estimation of C_{ant} storage rate for this layer is $188 \pm 21 \text{ kmol s}^{-1}$ which is not statistically different to the net C_{ant} input ($234 \pm 65 \text{ kmol s}^{-1}$). Therefore, we believe that the

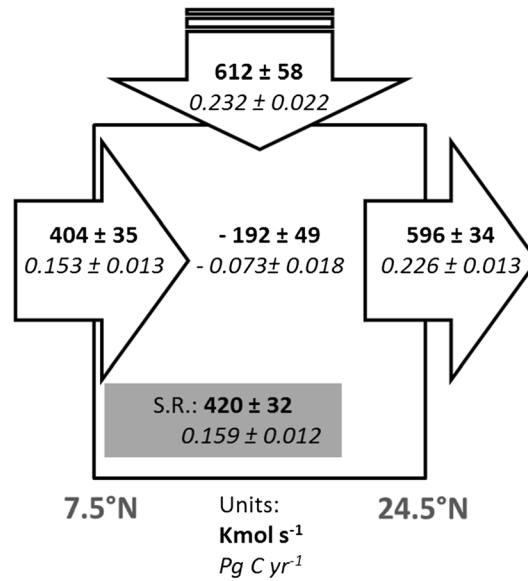


Figure 8. (a) C_{ant} balance for the whole TNA region referenced to 2001, the middle year of the studied period (1992–2011). Bold numbers are in kmol s^{-1} , and italic numbers are in Pg C yr^{-1} . The horizontal arrows stand for the C_{ant} transport across 7.5°N and 24.5°N . The numbers inside the box represent the net input of C_{ant} due to the lateral transport. The values inside the grey box correspond to the C_{ant} storage rate. The vertical arrow represents the air-sea transfer of C_{ant} as inferred from the C_{ant} balance.

meridional C_{ant} transport across $7.5^\circ\text{N}/24.5^\circ\text{N}$ sections ($493 \pm 51 \text{ kmol s}^{-1}/662 \pm 49 \text{ kmol s}^{-1}$) and the C_{ant} storage rate of the total volume of our TNA region ($489 \pm 32 \text{ kmol s}^{-1}$ or $0.18 \pm 0.012 \text{ Pg yr}^{-1}$; Table 4), the inferred air-sea exchange turns out to be $658 \pm 65 \text{ kmol s}^{-1}$ or $0.25 \pm 0.02 \text{ Pg yr}^{-1}$. This result is not much different to that computed considering only the upper layer.

The most striking results of our 2010–2011 C_{ant} budget are the high net input detected in the deep layer and the very high C_{ant} air-sea flux inferred for the TNA region. These results may be confirmed with those drawn from the 1992–1993 C_{ant} budget. Figure 7 also shows the mass and C_{ant} balance in the TNA during 1992–1993. As for 2010–2011, the mass conservation is also satisfied (Figure 7a). With regard to C_{ant} , the net input through lateral advection into the deep layer is $112 \pm 60 \text{ kmol s}^{-1}$. This estimate agrees with the C_{ant} storage rate referenced to 1993 ($139 \pm 21 \text{ kmol s}^{-1}$, Table 4). Consequently, our hypothesis that C_{ant} accumulation in the TNA deep layer is mainly due to the lateral advection is also supported by the 1992–1993 C_{ant} budget. Regarding the upper layer, during 1992–1993 there is a net loss of C_{ant} of $-327 \pm 61 \text{ kmol s}^{-1}$ due to lateral advection. Despite this net loss, the upper layer accumulates $215 \pm 24 \text{ kmol s}^{-1}$ of C_{ant} , similar to the value found during 2010–2011 ($291 \pm 24 \text{ kmol s}^{-1}$). Therefore, the inferred C_{ant} air-sea exchange necessary to compensate the 1992–1993 storage rate plus advective loss is $542 \pm 66 \text{ kmol s}^{-1}$ ($0.21 \pm 0.02 \text{ Pg yr}^{-1}$), a value similar to the one obtained for the 2010–2011 period. If instead of using only the upper layer we were to use the whole water volume in the TNA, the inferred C_{ant} air-sea exchange would be $576 \pm 73 \text{ kmol s}^{-1}$ ($0.22 \pm 0.03 \text{ Pg C yr}^{-1}$); this amount compensates for the lateral advection (-215 ± 66) and the C_{ant} accumulation ($361 \pm 32 \text{ kmol s}^{-1}$). Considering the balances for both periods (1992–1993 and 2010–2011), our best estimate for the C_{ant} air-sea exchange in the TNA is $0.23 \pm 0.02 \text{ Pg C yr}^{-1}$. Figure 8 shows the C_{ant} budget in the TNA considering the whole volume of water; it is referred to 2001 as it has been computed as the mean value of 1992 and 2010 budgets.

These results show similar processes occurring during 1992–1993 and 2010–2011: (i) most of the C_{ant} accumulation in the deep layer is explained by the inflow of C_{ant} -enriched NADW through the 24.5°N and the recirculation of NADW along the 7.5°N section; (ii) the Florida Current causes a huge export of C_{ant} toward the North; and (iii) the TNA is a region actively uptaking C_{ant} . The main difference between the

accumulation of C_{ant} in the TNA deep layer is mainly due to the southward transport of NADW, recently ventilated and relatively enriched in C_{ant} , along the subpolar and subtropical North Atlantic and its northward recirculation along 7.5°N .

The lateral advection of C_{ant} in the upper layer of the TNA region causes a net loss of $-412 \pm 70 \text{ kmol s}^{-1}$; this loss is due to the strong northward transport of the Florida Current which transports $1996 \pm 17 \text{ kmol s}^{-1}$. Moreover, the C_{ant} storage rate in this layer is $291 \pm 24 \text{ kmol s}^{-1}$. Summing up storage and net advective transport in the upper layer, we infer the C_{ant} air-sea exchange to be $703 \pm 74 \text{ kmol s}^{-1}$ ($0.27 \pm 0.03 \text{ Pg yr}^{-1}$), positive numbers meaning C_{ant} uptake by the ocean. Note that the above value for the C_{ant} air-sea exchange has been computed considering only the upper layer of the TNA, following the hypothesis that C_{ant} storage in the TNA deep layer is only related to lateral advection of C_{ant} and air-sea flux only affects the upper layer. Nevertheless, we may also calculate the C_{ant} air-sea exchange considering the whole water volume of our TNA region. Considering the

1992–1993 and 2010–2011 C_{ant} budgets is the magnitude of the net C_{ant} input (output) in the deep (upper) layer. In the case of the deep layer, we have detected a changing role in the exportation-accumulation of C_{ant} due to changes in the circulation pattern. This point is further discussed in the next section.

4. Discussion and Conclusions

The transport of C_{ant} across the Atlantic at 7.5°N has been estimated for the first time using in situ data. Our results show this transport to be northward, increasing from $315 \pm 47 \text{ kmol s}^{-1}$ in 1993 to $493 \pm 51 \text{ kmol s}^{-1}$ in 2010. Our results may be compared with estimates from ocean inverse models (combination of general circulation models with database of properties defining the CO_2 system): our results are quite similar to those obtained by Gruber *et al.* [2009], who estimated 370 kmol s^{-1} (referenced to 1995), or by DeVries [2014], where C_{ant} transport was computed to be $581 \pm 26 \text{ kmol s}^{-1}$ (referenced to 2012). Khatiwala *et al.* [2013] summarized the transport, storage, and air-sea flux of C_{ant} referenced to 2005 obtained from different ocean inverse models; they show that the transport of C_{ant} across 7.5°N ranges between 237 kmol s^{-1} and 486 kmol s^{-1} , in agreement with our estimates.

The difference in C_{ant} transport at 7.5°N between 1993 and 2010 is explained both by an increase in C_{ant} affecting mainly the thermocline water, and by changes in the circulation patterns. The northward C_{ant} transport in the upper layer increases mainly because of a C_{ant} rise, as the principal changes in the circulation of the upper layer only affect the AAIW, a water mass with moderate C_{ant} concentration ($15 \mu\text{mol kg}^{-1}$); therefore, a change in the mass transport of AAIW causes relatively small changes in the C_{ant} transport. In contrast, the large decrease in the southward mass transport of NADW causes a considerable decrease in the southward C_{ant} transport, even though the C_{ant} concentration within NADW is even smaller than within AAIW. Therefore, the 1993 to 2010 intensification in the northward transport of C_{ant} through 7.5°N is the outcome both of an increase in northward C_{ant} transport in the upper layer and a decrease in southward C_{ant} transport in the deep layer.

A novel aspect concerning the C_{ant} transport across the 24.5°N Atlantic section is the use of the same methodology for two different cruises. Therefore, our results allow a consistent analysis of the relative contribution of the changes in C_{ant} concentration and circulation to the variations in C_{ant} transport. The transport of C_{ant} increases from $530 \pm 46 \text{ kmol s}^{-1}$ in 1992 to $662 \pm 49 \text{ kmol s}^{-1}$ in 2011. The 1992 estimation is not statistically different from previous results obtained with in situ data: $449 \pm 158 \text{ kmol s}^{-1}$ [Macdonald *et al.*, 2003] or $610 \pm 200 \text{ kmol s}^{-1}$ [Rosón *et al.*, 2003]; the difference between previous estimates and our result lies on the uncertainties. The largest error was given by Rosón *et al.* [2003], because it was computed as the standard deviation of the random perturbation of both mass transport and C_{ant} concentration. Macdonald *et al.* [2003] took into account only the error associated to the mass transport, obtaining errors smaller than Rosón *et al.* [2003] yet larger than our results. Our error estimates are smaller than these previous results because our mass transports are computed using an inverse model with 17 layers applied to two transoceanic sections [Hernández-Guerra *et al.*, 2014], while Macdonald *et al.* [2003] consider a single layer throughout the 24.5°N section. Our results of C_{ant} transport across 24.5°N section are also in agreement with those obtained from a biogeochemical model, $396 \pm 106 \text{ kmol s}^{-1}$ referenced to the 1990s decade [Tjiputra *et al.*, 2010]. However, they do not agree with those deduced from ocean inverse models, which provide values significantly smaller. Gruber *et al.* [2009] estimated a C_{ant} transport of 211 kmol s^{-1} (referenced to 1995), or DeVries [2014] obtained a C_{ant} transport of $370 \pm 26 \text{ kmol s}^{-1}$ (referenced to 2012). Khatiwala *et al.* [2013] showed that C_{ant} transport across 24.5°N, as estimated by different ocean inverse models, ranges between 106 kmol s^{-1} and 181 kmol s^{-1} (referenced to 2005); these authors also showed that ocean inverse model estimates are 3 to 5 times smaller compared with C_{ant} transports computed from in situ data (see their Figure 6). The low C_{ant} transport at 24.5°N estimated by ocean inverse models is likely related to the model's inability to properly account for the intense northward C_{ant} transport by the Florida Current. This leads to very small C_{ant} output in the TNA, causing the C_{ant} air-sea flux to be underestimated by ocean inverse models.

A large part of the increase of C_{ant} transport across 24.5°N from 1992 to 2011 is caused by the C_{ant} increase undergone by the thermocline waters, essentially those transported by the Florida Current. The increase of C_{ant} transport by this current is 582 kmol s^{-1} , much larger than the net increase in C_{ant} transport through

the whole section (132 kmol s^{-1}). Consequently, the effect of the circulation on the C_{ant} transport changes cannot be neglected, yet it does not affect the Florida Current which mass transport shows low variability. The change in the circulation pattern between 1992 and 2011 causes a decrease in the northward C_{ant} transport, softening the meridional northward C_{ant} transport that would be reached in 2011 otherwise. Two behaviors explain the decreasing effect of the circulation changes on the C_{ant} transport: (i) the decrease in the net northward mass transport in the upper layer due to the larger southward transport east of the Florida's Strait and (ii) the increase in the southward transport of C_{ant} , as a result of a shift in the southward flow from C_{ant} -poor INADW in 1992 to C_{ant} -rich uNADW in 2011.

The second part of this paper aims at defining the C_{ant} budget in the TNA. A net input of C_{ant} has been detected in the deep layer as a result of more supply through the 24.5°N section than export through the 7.5°N section. The C_{ant} net input is $112 \pm 60 \text{ kmol s}^{-1}$ ($234 \pm 65 \text{ kmol s}^{-1}$) in 1992–1993 (2010–2011), not statistically different from C_{ant} storage rate in this layer, estimated as $139 \pm 21 \text{ kmol s}^{-1}$ ($188 \pm 21 \text{ kmol s}^{-1}$). These results confirm that the C_{ant} increase detected in the deep layer is due to both the large injection of recently ventilated C_{ant} -rich NADW across 24.5°N by the DWBC and the northward recirculation of this NADW at 7.5°N (Figures 5e and 6e). Furthermore, the role of the circulation changes on the accumulation of C_{ant} within the deep layer has also been identified. The AMOC slowdown observed from 1992–1993 to 2010–2011, with the decline of the southward mass transport across the 24.5°N and even further across 7.5°N , results in a change from exportation to accumulation within the deep TNA. During 1992–1993 the circulation is responsible for the export of 47–86% of the total C_{ant} entering the deep TNA. Contrarily, during 2010–2011, the advective C_{ant} export is reduced to only 27–50%. These results are due to changes in the circulation pattern.

The behavior in the TNA upper layer is quite different from that observed in the deep layer. We find C_{ant} net export due to lateral advection, yet an accumulation of C_{ant} is also detected in this layer. The air-sea transfer of C_{ant} , necessary to compensate for both net advective export and accumulation in the upper layer, is inferred here to be $0.27 \pm 0.03 \text{ Pg C yr}^{-1}$ ($0.21 \pm 0.02 \text{ Pg C yr}^{-1}$) during 2010–2011 (1992–1993). Since the C_{ant} air-sea fluxes cannot be measured directly, this result can only be compared with values inferred from ocean inverse models. *Mikaloff Fletcher et al.* [2006] inferred a C_{ant} air-sea flux of $0.04 \text{ Pg C yr}^{-1}$ referenced to 1995 or $0.05 \text{ Pg C yr}^{-1}$ referenced to 2010; *DeVries* [2014] estimated, referenced to 2012, a C_{ant} air-sea flux of $0.08 \text{ Pg C yr}^{-1}$. *Khaliwala et al.* [2013] found the C_{ant} air-sea fluxes in the TNA region, referenced to 2005, to range between $0.02 \text{ Pg C yr}^{-1}$ and $0.05 \text{ Pg C yr}^{-1}$ using ocean inverse model outputs which are referenced to 2005. All these estimates, rather similar between them, are as much as 1 order of magnitude smaller than our results.

For the whole volume of water, the C_{ant} storage rate is $0.159 \pm 0.010 \text{ Pg C yr}^{-1}$ (referenced to 2001, Table 4), which is larger than the results obtained from ocean inverse models [*Khaliwala et al.*, 2013], which range between 0.084 and $0.106 \text{ Pg C yr}^{-1}$ (rescaled to 2001). The difference is partially because we consider the Caribbean Sea, which is not included in the ocean inverse model estimates. If the Caribbean Sea is excluded, the C_{ant} storage rate is $0.123 \pm 0.008 \text{ Pg C yr}^{-1}$, yet about $0.03 \text{ Pg C yr}^{-1}$ larger than the ocean inverse models estimates. Furthermore, the C_{ant} storage rate along 7.5°N , observed by *Fajar et al.* [2015] using both TTD and ϕC_T^0 methods, is somehow larger than those estimated by the ocean inverse models. The discrepancy is likely caused by the rapid increase of the C_{ant} concentrations in 2010, due to the change in the ocean circulation.

The C_{ant} storage rates and lateral advection have been used to deduce the air-sea transfer of C_{ant} in the TNA region. Comparing our results with those obtained by ocean inverse models, we find good agreement in the C_{ant} transport across 7.5°N section, but our estimate for the C_{ant} transport across 24.5°N is about 500 kmol s^{-1} ($0.19 \text{ Pg C yr}^{-1}$) larger. We also find that our estimate for the C_{ant} storage rate is similar but moderately larger than obtained by the inverse models. Consequently, the small air-sea transfer of C_{ant} obtained from ocean inverse models is probably the result of the model's underestimation of the northward C_{ant} transport across the 24.5°N section.

The heat and C_{ant} budgets in the TNA are much related because of the following: (i) the AMOC transports warm C_{ant} -enriched water northward and returns colder and poorer in C_{ant} water southward, (ii) the tropical ocean uptakes heat and C_{ant} from the atmosphere, and (iii) the ocean is accumulating C_{ant}

[*Khaliwala et al.*, 2013] and heat [*Levitus et al.*, 2012]. Therefore, it is useful to also examine the heat budget for the TNA. Our estimates for the heat transport for the period 2010–2011 across 7.5°N and 24.5°N are 0.62 ± 0.06 PW and 1.23 ± 0.06 PW, respectively. Consequently, there is an advective heat loss of -0.61 ± 0.06 PW, mainly in the upper layer. The heat balance may still be modified by changes in heat content within the TNA; we can estimate these with the help of *Levitus et al.* [2012] observations for changes in the heat content in the upper 2000 m of the world ocean for the period 1955–2010. These authors found a heat content trend of $25 \times 10^{18} \text{ J yr}^{-1}$ (~ 0.0008 PW) for the TNA latitudes, which is very small compared to the lateral advection of heat. Hence, we can infer the heat air-sea exchange in the TNA to be 0.61 ± 0.06 PW, with positive numbers meaning heat uptake by the ocean. Following a similar procedure, we may calculate the heat air-sea exchange for the 1992–1993 period as 0.59 ± 0.05 PW. It turns out that both estimates of heat air-sea exchange are in agreement with available climatological values: according to *Josey et al.* [1999], the mean heat air-sea flux in the Atlantic 8–14°N and 14°–24°N bands is $44.6 \pm 10 \text{ W m}^{-2}$ which, when multiplied by the TNA surface area ($15.3 \times 10^{12} \text{ m}^2$), gives a heat air-sea exchange of 0.68 ± 0.16 PW, in very good agreement with our estimates. These results grant confidence to our estimates for CO₂ air-sea fluxes.

We are aware of the seasonality of mass transport across the 7.5°N section. The results presented here are obtained from single-cruise data, being hence unavoidably contaminated by the seasonal cycle, particularly because of the changes in wind forcing to the surface and upper thermocline waters and as a result of variations in mesoscale activity. Despite so, the good consistency in the C_{ant} and heat budgets for the upper ocean, as deduced from the two periods, together with the relative stability of the air-sea heat and gas exchange fluxes in the TNA [e.g., *Bunker* 1976], grant us confidence on the adequateness of the calculated results to characterize the C_{ant} budget in this region.

Summing up, the C_{ant} advective transport across the TNA is northward, acting as an important C_{ant} source to the subpolar North Atlantic. An increase in the northward transport of C_{ant} from 1992–1993 to 2010–2011 has been observed. This is mainly due to the C_{ant} increase in the thermocline water but attenuated by a weakening of the circulation. A large accumulation of C_{ant} has also been detected in the TNA deep layer, principally due to the southward advection of NADW recently ventilated in the subpolar North Atlantic and the recirculation of this water along the 7.5°N section. Finally, in spite of the large C_{ant} export from the TNA by the Florida Current, there is an important accumulation of C_{ant} in this basin, suggesting the C_{ant} uptake from the atmosphere to likely be much larger than previously suggested.

Acknowledgments

We thank the crew of *BIO Hespérides* and *R/V Sarmiento de Gamboa* and the scientific and technical teams for their support and essential help during the 2010 and 2011 cruises. We also wish to thank two anonymous reviewers for their suggestions and constructive comments. The first author received a grant from the Tricontinental Atlantic Campus spending a 6 month period at the Universidad de Las Palmas de Gran Canaria where this study was carried out. This work has been performed under the projects MOC2 (CTM2008-06438), Malaspina (CSD2008-00077), BOCATS (CTM2013-41048-P), and TIC-MOC (CTM2011-28867) supported by the Spanish Government and cofounded by the European Regional Development Fund (FEDER). We acknowledge David Sosa Trejo for his technical support in preparing the figures of this paper. The data used in this study are archived at the Carbon Dioxide Information Analysis Center (CDIAC), <http://cdiac.ornl.gov/oceans/RepeatSections>.

References

- Álvarez, M., A. F. Ríos, F. F. Pérez, H. L. Bryden, and G. Rosón (2003), Transports and budgets of total inorganic carbon in the subpolar and temperate North Atlantic, *Global Biogeochem. Cycles*, 17(1), 1002, doi:10.1029/2002GB001881.
- Antonov, J. I., D. Seidov, T. P. Boyer, R. A. Locarnini, A. V. Mishonov, H. E. Garcia, O. K. Baranova, M. M. Zweng, and D. R. Johnson (2010), *World Ocean Atlas 2009, Volume 2: Salinity*, NOAA Atlas NESDIS 69, edited by S. Levitus, 184 pp., U.S. Gov. Print. Off., Washington, D. C.
- Arhan, M., H. Mercier, B. Bourlès, and Y. Gouriou (1998), Hydrographic sections across the Atlantic at 7°30N and 4°30S, *Deep Sea Res., Part I*, 45, 829–872.
- Bunker, A. F. (1976), Computations of surface energy flux and annual air-sea interaction cycles of the North Atlantic, *Mon. Weather Rev.*, 104, 1122–1140.
- DeVries, T. (2014), The oceanic anthropogenic CO₂ sink: Storage, air-sea fluxes, and transports over the industrial era, *Global Biogeochem. Cycles*, 28, 631–647, doi:10.1002/2013GB004739.
- Fajar, N. M., E. F. Guallart, R. Steinfeldt, A. F. Ríos, J. L. Pelegrí, C. Pelejero, E. Calvo, and F. F. Pérez (2015), Anthropogenic CO₂ changes in the Equatorial Atlantic Ocean, *Prog. Oceanogr.*, doi:10.1016/j.pocean.2015.02.004.
- Fraile-Nuez, E., and A. Hernández-Guerra (2006), Wind-driven circulation for the eastern North Atlantic Subtropical Gyre from Argo data, *Geophys. Res. Lett.*, 33, L03601, doi:10.1029/2005GL025122.
- Ganachaud, A. (1999), Large scale oceanic circulation and fluxes of freshwater, heat, nutrients and oxygen, PhD thesis (These), Massachusetts Institute of Technology/ Wood Hole Oceanography Institution Joint Program.
- Gruber, N., J. L. Sarmiento, and T. F. Stocker (1996), An improved method for detecting anthropogenic CO₂ in the oceans, *Global Biogeochem. Cycles*, 10, 809–837.
- Gruber, N., et al. (2009), Oceanic sources, sinks, and transport of atmospheric CO₂, *Global Biogeochem. Cycles*, 23, GB1005, doi:10.1029/2008GB003349.
- Guallart, F., et al. (2015), Trends in anthropogenic CO₂ in water masses of the subtropical North Atlantic Ocean, *Prog. Oceanogr.*, 131, 21–32, doi:10.1016/j.pocean.2014.11.006.
- Hernández-Guerra, A., J. L. Pelegrí, E. Fraile-Nuez, V. Benítez-Barrios, M. Emelianov, M. D. Pérez-Hernández, and P. Véllez-Belchí (2014), Meridional overturning transports at 7.5N and 24.5N in the Atlantic Ocean during 1992–93 and 2010–11, *Prog. Oceanogr.*, 128, 98–114, doi:10.1016/j.pocean.2014.08.016.
- Jackett, D. R., and T. J. McDougall (1997), A neutral density variable for the world's oceans, *J. Phys. Oceanogr.*, 27, 237–263, doi:10.1175/1520-0485(1997)027<0237:ANDVFT>2.0.CO;2.
- Josey, S. A., E. C. Kent, and P. K. Taylor (1999), New insights into the ocean heat budget closure problem from analysis of the SOC air-sea flux climatology, *J. Clim.*, 12, 2856–2880.

- Khatiwala, S., F. Primeau, and T. Hall (2009), Reconstruction of the history of anthropogenic CO₂ concentration in the ocean, *Nature*, *462*, 346–349, doi:10.1038/nature08526.
- Khatiwala, S., et al. (2013), Global ocean storage of anthropogenic carbon, *Biogeosciences*, *10*, 2169–2191, doi:10.5194/bg-10-2169-2013.
- Lavin, A., H. L. Bryden, and G. Parrilla (1998), Meridional transport and heat flux variations in the subtropical North Atlantic, *Global Atmos. Ocean Syst.*, *6*, 269–293.
- Levitus, S., et al. (2012), World ocean heat content and thermosteric sea level change (0–2000 m), 1955–2010, *Geophys. Res. Lett.*, *39*, L10603, doi:10.1029/2012GL051106.
- Locarnini, R. A., A. V. Mishonov, J. I. Antonov, T. P. Boyer, H. E. Garcia, O. K. Baranova, and M. M. Zweng (2010), in *World Ocean Atlas 2009, Volume 1: Temperature*, NOAA Atlas NESDIS, vol. 68, edited by S. Levitus, 184 pp., U.S. Gov. Print. Off., Washington, D. C.
- Lux, M., H. Mercier, and M. Arhan (2001), Interhemispheric exchanges of mass and heat in the Atlantic Ocean in January–March 1993, *Deep Sea Res., Part I*, *48*, 605–638.
- Macdonald, A. (1995), Oceanic fluxes of mass, heat and freshwater: A global estimate and perspective, PhD thesis, Mass. Inst. of Technol./Woods Hole Oceanogr. Inst. Joint Program, Cambridge, 1995. Massachusetts Institute of Technology/Woods Hole Oceanography Institution Joint Program.
- Macdonald, A. M., M. O. Baringer, R. Wanninkhof, K. Lee, and D. W. Wallace (2003), A 1998–1992 comparison of inorganic carbon and its transport across 24.5°N in the Atlantic, *Deep Sea Res., Part II*, *50*, 3041–3064, doi:10.1016/j.dsr2.2003.07.009.
- McCartney, M. S., and L. D. Talley (1982), The subpolar mode water of the North Atlantic Ocean, *J. Phys. Oceanogr.*, *12*, 1169–1188.
- Mikaloff Fletcher, S. E., et al. (2006), Inverse estimates of anthropogenic CO₂ uptake, transport, and storage by the ocean, *Global Biogeochem. Cycles*, *20*, GB2002, doi:10.1029/2005GB002530.
- Oudot, C., J.-F. Ternon, and J. Lecomte (1995), Measurements of atmospheric and oceanic CO₂ in the tropical Atlantic: 10 years after the 1982–1984 FOCAL cruises, *Tellus B*, *47*, 70–85.
- Oudot, C., P. Morin, F. Baurand, M. Wafar, and P. L. Corre (1998), Northern and southern water masses in the equatorial Atlantic distribution of nutrients on the WOCE A6 and A7 lines, *Deep Sea Res., Part I*, *45*, 873–902.
- Pérez, F. F., H. Mercier, M. Vázquez-Rodríguez, P. Lherminier, A. Velo, P. C. Pardo, G. Rosón, and A. F. Ríos (2013), Atlantic Ocean CO₂ uptake reduced by weakening of the meridional overturning circulation, *Nat. Geosci.*, *6*, 146–152, doi:10.1038/NGEO1680.
- Rhein, M., D. Kieke, and R. Steinfeldt (2007), Ventilation of the Upper Labrador Sea Water, 2003–2005, *Geophys. Res. Lett.*, *34*, L06603, doi:10.1029/2006GL028540.
- Ríos, A. F., F. F. Pérez, J. L. Pelegrí, and N. Fajar (2012), Carbon data obtained during the R/V *Hesperides* cruise in the Atlantic Ocean on CLIVAR repeat hydrography section A06, (5 April–16 May, 2010).
- Rosón, G., A. F. Ríos, F. F. Pérez, A. Lavin, and H. L. Bryden (2003), Carbon distribution, fluxes, and budgets in the subtropical North Atlantic Ocean (24.5°N), *J. Geophys. Res.*, *108*(C5), 3144, doi:10.1029/1999JC000047.
- Sabine, C. L., et al. (2004), The oceanic sink for anthropogenic CO₂, *Science*, *305*, 367–371, doi:10.1126/science.1097403.
- San Antolín Plaza, M. Á., J. L. Pelegrí, F. J. Machin, and V. Benítez Barrios (2012), Inter-decadal changes in stratification and double diffusion in a transatlantic section along 7.5°N, *Sci. Mar.*, *76*, 189–207, doi:10.3989/scimar.03616.19G.
- Steinfeldt, R., M. Rhein, J. L. Bullister, and T. Tanhua (2009), Inventory changes in anthropogenic carbon from 1997–2003 in the Atlantic Ocean between 20°S and 65°N, *Global Biogeochem. Cycles*, *23*, GB3010, doi:10.1029/2008GB003311.
- Stramma, L., and F. Schott (1999), The mean flow field of the tropical Atlantic Ocean, *Deep Sea Res., Part II*, *46*, 279–304, doi:10.1016/S0967-0645(98)00109-X.
- Tanhua, T., A. Biastoch, A. Körtzinger, H. Lüger, C. Böning, and D. W. Wallace (2006), Changes of anthropogenic CO₂ and CFCs in the North Atlantic between 1981 and 2004, *Global Biogeochem. Cycles*, *20*, GB4017, doi:10.1029/2006GB002695.
- Tjiputra, J. F., K. Assmann, and C. Heinze (2010), Anthropogenic carbon dynamics in the changing ocean, *Ocean Sci.*, *6*, 605–614, doi:10.5194/os-6-605-2010.
- Touratier, F., L. Azouzi, and C. Goyet (2007), CFC-11, Δ14C and 3H tracers as a means to assess anthropogenic CO₂ concentrations in the ocean, *Tellus B*, *59*, 318–325, doi:10.1111/j.1600-0889.2006.00247.x.
- Vázquez Rodríguez, M., F. Touratier, C. Lo Monaco, D. W. Waugh, X. A. Padin, R. G. J. Bellerby, C. Goyet, N. Metzl, A. F. Ríos, and F. F. Pérez (2009), Anthropogenic carbon distributions in the Atlantic Ocean: Data-based estimates from the Arctic to the Antarctic, *Biogeosciences*, *6*, 439–451. [Available at <http://www.biogeosciences.net/6/439/2009/>.]
- Waugh, D. W., T. W. N. Haine, and T. M. Hall (2004), Transport times and anthropogenic carbon in the subpolar North Atlantic Ocean, *Deep Sea Res., Part I*, *51*, 1475–1491, doi:10.1016/j.dsr.2004.06.011.
- Waugh, D. W., T. M. Hall, B. I. McNeil, R. Key, and R. J. Matear (2006), Anthropogenic CO₂ in the oceans estimated using transit time distributions, *Tellus B*, *58*, 376–389, doi:10.1111/j.1600-0889.2006.00222.x.
- Zunino, P., M. I. García-Ibanez, P. Lherminier, H. Mercier, A. F. Ríos, and F. F. Pérez (2014), Variability of the transport of anthropogenic CO₂ at the Greenland-Portugal OVIDE section: Controlling mechanisms, *Biogeosciences*, *11*, 2375–2389, doi:10.5194/bg-11-2375-2014.